Partially Folded Intermediates in Insulin Fibrillation†

Atta Ahmad,‡ Ian S. Millett,§ Sebastian Doniach,§ Vladimir N. Uversky,‡ and Anthony L. Fink*,‡

Department of Chemistry and Biochemistry, University of California, Santa Cruz, California 95064, and Departments of Physics and Chemistry, Stanford University, Stanford, California 94305

Received May 23, 2003

ABSTRACT: Native zinc-bound insulin exists as a hexamer at neutral pH. Under destabilizing conditions, the hexamer dissociates, and is very prone to forming fibrils. Insulin fibrils exhibit the typical properties of amyloid fibrils, and pose a problem in the purification, storage, and delivery of therapeutic insulin solutions. We have carried out a systematic investigation of the effect of guanidine hydrochloride (Gdn·HCl)-induced structural perturbations on the mechanism of fibrillation of insulin. At pH 7.4, the addition of as little as 0.25 M Gdn·HCl leads to dissociation of insulin hexamers into dimers. Moderate concentrations of Gdn·HCl lead to formation of a novel partially unfolded dimer state, which dissociates into a partially unfolded monomer state. High concentrations of Gdn·HCl resulted in unfolded monomers with some residual structure. The addition of even very low concentrations of Gdn·HCl resulted in substantially accelerated fibrillation, although the yield of fibrils decreased at high concentrations. Accelerated fibrillation correlated with the population of the expanded (partially folded) monomer, which existed up to >6 M Gdn·HCl, accounting for the formation of substantial amounts of fibrils under such conditions. In the presence of 20% acetic acid, where insulin exists as the monomer, fibrillation was also accelerated by Gdn·HCl. The enhanced fibrillation of the monomer was due to the increased ionic strength at low denaturant concentrations, and due to the presence of the partially unfolded, expanded conformation at Gdn·HCl concentrations above 1 M. The data suggest that under physiological conditions, the fibrillation of insulin involves both changes in the association state (with rate-limiting hexamer dissociation) and conformational changes, leading to formation of the amyloidogenic expanded monomer intermediate.

The importance of conformational switches in proteins leading to disease states is increasingly recognized and has been well documented (*1*−*6*). Among the various pathological forms resulting from changes in the native conformation, the formation of "amyloid" has attracted the most attention. Amyloid deposits from different tissue systems exhibit a similar submicroscopic structure consisting of linear fibrils ranging in width from 60 to 130 Å and in length from 1 to 16 μm (*7*, *8*); invariably, nonprotein and nonfibrillar components are also found in amyloid deposits (*9*). Although amyloid deposits are extracellular, similar fibrils are also found in intracellular deposits in diseases such as Parkinson's and Huntington's diseases.

Protein fibrils are stained with the dyes Congo red and thioflavin T (*10*), and exhibit a characteristic cross-β structure in fiber diffraction studies; i.e., the β-strands are perpendicular to the fibril axis, and stack into axially aligned extended β-sheets (*11*, *12*). Protein fibrillation is not limited to disease-causing proteins; proteins that are not amyloidogenic have also been found to undergo self-assembly under various destabilizing conditions (*13*). Several hypotheses and models have been proposed for the mechanism of fibril formation; all these models have in common the need for a structural change in the native state as a requirement for fibril formation, and thus, the resultant diseases are considered protein conformational disorders (*1*, *14*).

Insulin, a 51-residue hormone, undergoes fibrillation under various conditions *in vitro* (*15*, *16*). Amyloid deposits of insulin have been observed both in patients with type II diabetes and in normal aging, as well as after subcutaneous insulin infusion and after repeated injection (*17*, *18*). Insulin fibrillation poses a variety of problems, including in the production, storage, and delivery (especially via insulin pumps) of soluble insulin.

Insulin exists in equilibrium as a mixture of monomer, dimer, hexamer, and possibly higher oligomeric states in solution, but the physiologically predominant storage form is a 2Zn-coordinated hexamer formed by association of three insulin dimers (*18*). Monomeric insulin exists in the R or T state, differing in the length of the α-helix in the B chain. Upon destabilization by temperature, low pH, organic solvents, or hydrophobic surfaces, insulin is highly susceptible to fibril formation (*15*, *16*, *18*−*20*). It has been noted that urea increased the rate of insulin fibrillation, whereas stabilizers such as TMAO and sucrose decreased it (*16*). It has been proposed that insulin fibrillation occurs through the dissociation of oligomers into monomer and the monomer undergoes a structural change, developing a strong propensity for fibrillation (*15*, *16*, *18*, *21*−*23*).

† This research was supported in part by a grant from UC BioSTAR and Novo Nordisk A/S to A.L.F.

* To whom correspondence should be addressed: Department of Chemistry and Biochemistry, University of California, Santa Cruz, CA 95064. Telephone: (831) 459-2744. Fax: (831) 459-2935. E-mail: fink@chemistry.ucsc.edu or uversky@hydrogen.ucsc.edu.

‡ University of California.

§ Stanford University.

10.1021/bi034868o CCC: $25.00
Published on Web 09/10/2003

In this investigation, we studied the relation between various insulin conformations, induced by guanidine hydrochloride (Gdn·HCl), with their propensity to fibrillate, both under physiological conditions (pH 7.4) starting with the hexamer and under conditions where the insulin monomer was the stable starting state (20% acetic acid) (*24*, *25*). Structural changes were monitored by optical spectroscopy, size-exclusion chromatography, and X-ray scattering; fibril formation was monitored by a thioflavin T fluorescence assay (*26*) and electron microscopy. The results indicate a marked influence of Gdn·HCl on the quaternary, tertiary, and secondary structure and fibrillation of insulin.

EXPERIMENTAL PROCEDURES

Materials

Chemicals. Human insulin with zinc was provided by Novo Nordisk (Copenhagen, Denmark). All the chemicals were analytical grade, and were from EM Sciences or Sigma. Thioflavin T was obtained from Fluka.

Preparation of Samples. Stock solutions of human insulin (2−10 mg/mL) were prepared fresh before being used in 0.025 M HCl (pH 1.6). For experiments starting with hexameric insulin, aliquots of 1 M HEPES buffer were added to obtain a final concentration of 50 mM and the pH was adjusted to 7.4 using NaOH. For studies of monomeric insulin, a stock solution was freshly prepared by dissolving human insulin in 20% acetic acid. The concentration of insulin was checked by using an extinction coefficient of 1.0 for 1 mg/mL at 276 nm (*16*). The concentration of Gdn·HCl solutions was obtained by refractive index measurements. Stock (1 mM) solutions of thioflavin T were prepared by dissolving ThT[1] in double-distilled water, and the concentration was determined using a molar extinction coefficient of 24 420 at 420 nm. ThT was stored at 4 °C, protected from light.

The effect of Gdn·HCl was studied by mixing aliquots from all the stock solutions to reach final concentrations of 2 mg/mL protein, 50 mM HEPES, and 20 μM ThT and a Gdn·HCl concentration varying from 0 to 6 M. In the case of the studies at pH 2, aliquots were added to each sample to reach final concentrations of 20% acetic acid, 2 mg/mL human insulin, and 20 μM ThT and a Gdn·HCl concentration varying from 0 to 6 M.

Methods

Kinetic Studies. The ThT fluorescence was monitored for each sample in a 96-well plate in a Fluoroskan Ascent CF fluorescence plate reader (Lab Systems) at 37 or 40 °C with 760 rpm shaking. The plate was sealed with Mylar plate sealer (Thermo Labsystems). The excitation wavelength was 444 nm and the emission measured at 485 nm. Plates were continuously shaken for the entire period of study at a rotation diameter of 1 mm, and the integration period was fixed at 20 ms for each well. Five replicates, corresponding to five wells for each sample, were used to minimize well-to-well variation. Results from more than three similar profiles were averaged for the final results at each Gdn·HCl concentration. The profiles obtained from kinetic analysis were curve-fitted using SigmaPlot software (*16*).

Circular Dichroism. CD spectra were recorded at 25 °C on an AVIV 60DS circular dichroism spectrophotometer (Aviv Associates, Lakewood, NJ). Aliquots from stock solutions were mixed to a final concentration of 2 mg/mL human insulin and a Gdn·HCl concentration varying from 0 to 6 M. To eliminate contributions from buffer, solutions without protein were prepared in the same manner described above and their spectra subtracted from the protein spectra. Samples were incubated for 2 h before the spectra were collected. Both near- and far-UV spectra were recorded using a step size of 0.5 nm and a bandwidth of 1.5 nm. In the far-UV region, spectra were recorded in a 0.01 cm cell; for the near-UV experiments, a cell with a path length of 0.5 cm was used.

Analysis of Spectroscopic Data (Phase Diagrams). The "phase diagram" method analysis of spectroscopic data is extremely sensitive to the detection of intermediate states (*27*−*31*). It is important to note that only *extensive* parameters (i.e., those parameters whose value is proportional to the amount of the analyzed matter in a system) should be used for such an analysis. The essence of the phase diagram method is to build up the diagram of $I(\lambda_1)$ *versus* $I(\lambda_2)$, where $I(\lambda_1)$ and $I(\lambda_2)$ are the spectral intensity values measured at wavelengths λ_1 and λ_2, respectively, under different experimental conditions for a protein undergoing structural transformations. In application to protein unfolding, the relation $I(\lambda_1) = f[I(\lambda_2)]$ will be linear if changes in the protein environment lead to an all-or-none transition between two different conformations. In contrast, the nonlinearity of this function reflects the sequential character of structural transformations, where each linear portion of the $I(\lambda_1) = f[I(\lambda_2)]$ plot describes an individual all-or-none transition. In principle, λ_1 and λ_2 are arbitrary wavelengths of the spectrum, but in practice, such diagrams are more informative if λ_1 and λ_2 are on different slopes of the spectrum. If the wavelengths are from one slope or near the maximum, some transitions may remain undetected.

Small-Angle X-ray Scattering. Small-angle X-ray scattering measurements were taken using the SAXS setup at beamline 4-2 at the Stanford Synchrotron Radiation Laboratory. Scattering patterns were recorded by a linear position-sensitive proportional counter, which was filled with an 80% Xe/20% CO_2 gas mixture. Scattering patterns were normalized by incident X-ray intensity, which was measured with a short length ion chamber before the sample. The sample-to-detector distance was calibrated to be 230 cm, using a cholesterol myristate sample. To avoid radiation damage of the sample, the protein solution was continuously passed through a 1.3 mm path length observation flow cell with 25 μm mica windows. Background measurements were performed before and after each protein measurement and then averaged before being used for background subtraction. All SAXS measurements were performed at 25 °C. The instrument calibration was checked by cytochrome *c*. The values for the radii of gyration (R_g) were calculated according to the Guinier approximation (*32*).

$$\ln I(Q) = \ln I(0) - R_g^2 Q^2/3$$

[1] Abbreviations: CD, circular dichroism; FTIR, Fourier transform infrared; ThT, thioflavin T; SEC, size-exclusion chromatography; SAXS, small-angle X-ray scattering.

where Q is the scattering vector given by the equation $Q = (4\pi \sin \theta)/\lambda$ (2θ is the scattering angle and λ is the wavelength of the X-ray). The value of $I(0)$, the forward scattering amplitude $I(Q)(Q \rightarrow 0)$, is proportional to the square of the molecular mass of the molecule (*32*). $I(0)$ for a pure dimer sample will therefore be twice that for a sample with the same number of monomers since each dimer will scatter 4 times as strongly, but there will be half as many as in the pure monomer sample.

Size-Exclusion Chromatography. Size-exclusion chromatography was performed using a Superose 12 HR 10/30 column from Pharmacia Biotech. (exclusion limit of $2 \times 10^6 M_r$). The column was run on an FPLC GP 250-P500 (Pharmacia Biotech) instrument at a flow rate of 0.4 mL/min with detection at 280 nm. Human insulin (2 mg/mL) was incubated in 50 mM HEPES (pH 7.4) with and without increasing concentrations of Gdn·HCl for 2 h at 25 °C. Two hundred microliters of each sample was loaded on the column. The column was equilibrated with 50 mM HEPES buffer containing the desired concentration of Gdn·HCl prior to the loading of sample. For experiments involving different insulin concentrations, 0.5−10 mg/mL insulin was incubated in 2.0 M Gdn·HCl and 50 mM HEPES (pH 7.4) for 2 h at 25 °C, and 200 μL of this solution was loaded on the column pre-equilibrated with 2.0 M Gdn·HCl and 50 mM HEPES (pH 7.4).

Aprotonin ($M_r = 6.5$ kDa) and cytochrome *c* ($M_r = 12.3$ kDa) were run as markers in the presence of 0.5 M Gdn·HCl and 50 mM HEPES (pH 7.4). Since no significant changes in these proteins have been observed in 0.5 M Gdn·HCl, these markers were assumed to be globular under these conditions. The observed elution volumes of 15.0 and 14.0 mL (data not shown) for aprotonin and cytochrome *c*, respectively, are consistent with their size.

Calculation of Fractions of Intermediates. The fractions of expanded dimers and expanded monomers were calculated from the SEC−HPLC data. The fraction of expanded dimers was calculated as the difference between the curve representing the decrease in the fraction of compact dimers and the curve representing the disappearance of expanded dimers (the second transition in the fraction of monomers, Figure 4B). The fraction of expanded monomers was calculated from the difference between the curve representing the decrease in the fraction of compact monomers (coincident with the curve for the disappearance of compact dimers, etc.) and the curve representing unfolding (the second transition in the elution volume of monomers, Figure 4A). Both fractions were scaled according to the population of monomers and dimers at 2.5 M Gdn·HCl (Figure 4B).

UV Absorbance Studies. Human insulin (2 mg/mL) was prepared and incubated in wells in the fluorescence plate reader as discussed above; however, ThT at a final concentration of 20 μM was added to only one of the five wells and was taken as a reference to monitor formation of fibrils. Once the transition into fibrils was complete, the contents from each of the wells were transferred to 0.5 mL centrifuge tubes and centrifuged at 14 000 rpm for 15 min. The supernatant was carefully removed, and the absorbance for the protein or ThT was measured. For the protein, 50 μL of the supernatant was dissolved in 950 μL of 25 mM HCl and 0.1 M NaCl (pH 2.0). The percentage of protein left in the supernatant was calculated by taking the absorbance of 2.0 mg/mL protein in 50 mM HEPES (pH 7.4), processed in a similar manner (50 μL in buffer), to be 100%. For samples in 20% acetic acid, the pellet obtained as described above was dissolved in 600 mM NaOH and the absorbance read at 290 nm.

Transmission Electron Microscopy. Aliquots of 5 μL of insulin fibrils grown in microplates without ThT at 2 mg/mL were diluted once, and 5 μL of the resulting solution was placed onto carbon grids coated with Formvar (Ted Pella Inc.) and left for 1−5 min. The grid was washed five times with nano-pure water and five times with 1% uranyl acetate for negative staining and left to dry at room temperature. The specimens were viewed and images recorded with a Philips 208 electron microscope operated at 80 kV using gatan digital micrography software.

Acrylamide Quenching. Tyrosine fluorescence quenching experiments were carried out on insulin solutions at 25 °C. A 2 mg/mL insulin stock solution was prepared in 20% acetic acid. Aliquots to give a final concentration of 0.1 mg/mL (~1 μM) were added to the solutions containing varying Gdn·HCl concentrations. Samples were incubated for 2 h before the fluorescence measurements were taken. For each sample, aliquots from an acrylamide stock (4.0 M) were added with a Hamilton syringe to reach a final concentration of acrylamide varying from 0 to 175 mM, and the fluorescence was measured immediately. The samples were excited at 276 nm, and emission was monitored at 301 nm.

RESULTS

Conformational transitions and fibrillation of insulin as a function of Gdn·HCl concentration were monitored at neutral pH, where insulin is hexameric, and in 20% acetic acid, where it is monomeric. Previous studies (*16*, *33*) have shown that dissociation of the hexamer is at least partially rate-limiting in fibrillation.

Structural Changes in Insulin Induced by Gdn·HCl at pH 7.4 Monitored by Circular Dichroism. Changes in the near-UV CD region of insulin were used to gain information about the quaternary and tertiary structure (*31*). The native hexameric protein exhibits a broad negative peak with a minimum at 276 nm, characteristic of tyrosine (there are no tryptophan residues in insulin). The addition of Gdn·HCl resulted in significant changes in the spectral shape and intensity (Figure 1A). A major transition was observed over the range of 0−3.5 M, with a midpoint of ~1.5 M; at higher Gdn·HCl concentrations, only gradual changes occur up to 6.25 M (Figure 1C). The spectra reveal that there is still tertiary structure present in 6.25 M Gdn·HCl. These observations show a constantly changing tyrosine environment as a function of Gdn·HCl concentration, but whether these changes reflect quaternary or tertiary structural disruptions cannot be determined from these data alone.

Far-UV CD spectra obtained under similar conditions are shown in Figure 1B. The native protein exhibits a spectrum typical of an α-helical protein, with characteristic minima at 222 and 209 nm. Although only small changes are observed in the vicinity of 222 nm within the Gdn·HCl concentration range of 0.5−2.5 M, significant changes are observed at 209 nm. As the Gdn·HCl concentration is increased further marked changes in both regions are observed until a spectrum representing the predominantly

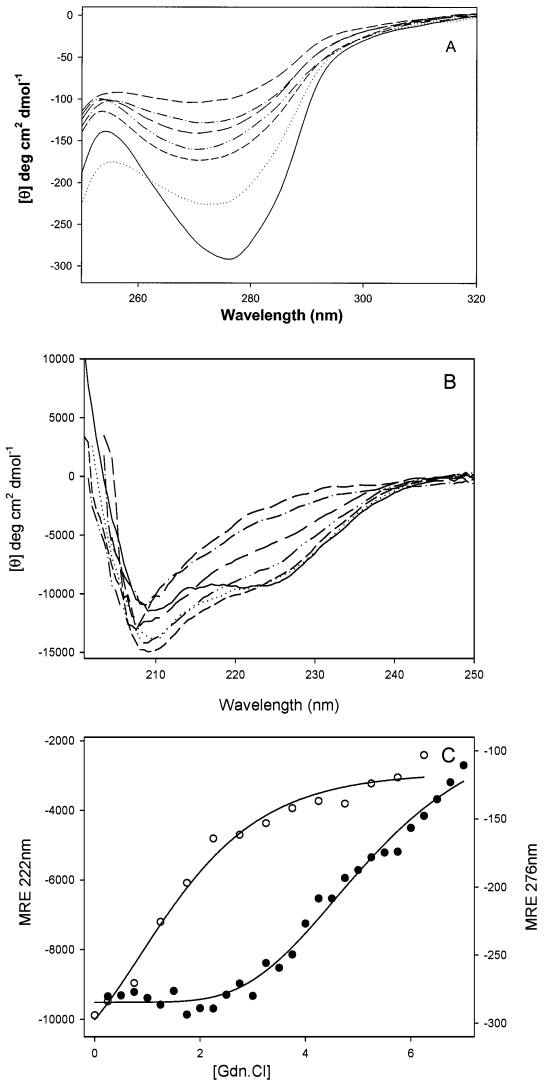

FIGURE 1: Effect of Gdn·HCl on hexameric insulin, monitored by circular dichroism. Panel A shows selected near-UV CD spectra; panel B shows selected far-UV CD spectra, and panel C shows the Gdn·HCl dependence of ellipticity at 222 (●) and 276 nm (○). Conditions were as follows: 2.0 mg/mL insulin, pH 7.4, and 25 °C. Each spectrum is the average of two independently collected spectra. In panel A, the Gdn·HCl concentrations are, from bottom to top, 0, 1.25, 2.25, 3.25, 4.25, 5.25, and 6.25 M. In panel B, the Gdn·HCl concentrations are, in order of decreasing ellipticity at 222 nm, 0, 1.0, 2.0, 3.0, 4.0, 5.0, 6.0, and 7.0 M.

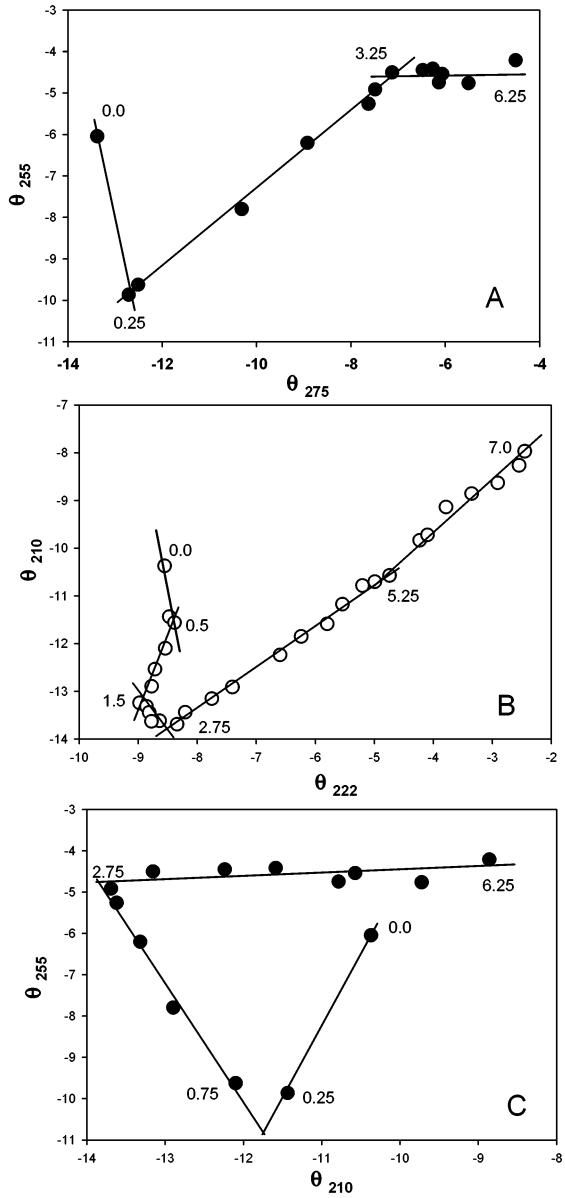

FIGURE 2: Phase diagrams (see the text) indicate multiple transitions in the Gdn·HCl-induced unfolded form of hexameric insulin. The graphs were obtained by plotting the ellipticities at 255 and 275 nm for near-UV CD (A) and 222 and 210 nm for far-UV CD (B). Panel C shows the phase diagram depicting the simultaneous changes in both far- and near-UV CD, reflecting simultaneous secondary structure and quaternary or tertiary structure. The numbers in each plot correspond to the Gdn·HCl concentrations at the nearest point. Conditions were as described in the legend of Figure 1.

unfolded form is obtained at 7.0 M Gdn·HCl. The shape of the spectrum at 7.0 M suggests the existence of some residual secondary structure, consistent with reports of stable super-secondary structure of the B chain from other studies (*34*).

Traditionally, CD data have been analyzed in terms of fraction folded/unfolded *versus* Gdn·HCl concentration (Figure 1C), but we found that phase diagrams were more informative in this case. Phase diagrams have been used to resolve complex structural changes from both fluorescence and CD data (*29*−*31*). Figure 2A represents the phase diagram obtained by plotting the ellipticity at 275 nm *versus* that at 255 nm; these wavelengths were chosen on the basis of the significant changes in ellipticity in Figure 1A. This phase diagram shows three linear segments (from 0 to 0.25 M Gdn·HCl, from 0.25 to 3.25 M Gdn·HCl, and from 3.25 to 6.25 M Gdn·HCl). Each change in slope corresponds to a different structural transition; thus, there are four distinct structural species. As will be discussed later, these species correspond to the starting hexamer, the compact dimer and monomer, expanded (partially unfolded intermediate) dimers and monomers, and the unfolded monomer, respectively.

The corresponding phase diagram for the far-UV CD data, obtained by plotting ellipticities at 222 nm *versus* those at 210 nm (Figure 2B), shows five sets of structural changes as depicted by the different linear segments ranging from 0 to 0.5 M Gdn·HCl, from 0.5 to 1.5 M Gdn·HCl, from 1.5 to 2.75 M Gdn·HCl, from 2.75 to 5.25 M Gdn·HCl, and from 5.25 to 7.0 M Gdn·HCl. Unlike the near-UV CD-based tertiary structure data, the secondary structure of insulin seems to undergo more complex alterations with multiple

transitions. On the basis of subsequent data, the major species responsible for these transitions are the hexamer, the compact and expanded dimer, the compact and expanded monomer, and the unfolded monomer.

To obtain a correlation between the changes in secondary and tertiary or quaternary structures, a phase diagram was obtained as a θ_{255} *versus* θ_{210} plot (Figure 2C). This plot shows a first transition extending from 0 to 0.25 M Gdn·HCl, followed by a second transition from 0.75 to 2.75 M Gdn·HCl, which in turn is followed by a third transition from 2.75 to 6.25 M Gdn·HCl. On the basis of additional data, these transitions reflect dissociation of the hexamer, changes from a mixture of compact to expanded dimeric and monomeric species (see Figure 13B), and formation of unfolded monomers.

The data in Figure 2 indicate that the Gdn·HCl-induced unfolding of human insulin at pH 7.4 is a very complex process. Interestingly, Figure 2C shows at least two conformational transitions that are accompanied by simultaneous changes in quaternary or tertiary and secondary structure, at 0.5 and 2.75 M Gdn·HCl; these correspond to loss of hexamers, and dimeric species, respectively.

Structural Changes in Insulin Induced by Gdn·HCl at pH 7.4 Monitored by Size-Exclusion Chromatography. Samples of insulin were incubated at pH 7.4 in the presence and absence of the desired Gdn·HCl concentrations for 2 h before being injected onto the Superose S12 column, equilibrated in the same concentration of Gdn·HCl. Figure 3A summarizes the results of size-exclusion chromatography. Native insulin exhibited an elution volume of 6.1 mL, corresponding to the hexamer. However, in the presence of low Gdn·HCl concentrations, insulin eluted at larger elution volumes. At the lowest Gdn·HCl concentrations, the position of the peak corresponded to the molecular mass of dimeric insulin (11.6 kDa), with a small shoulder corresponding to the monomeric (5.8 kDa) form of insulin, indicating dissociation of the insulin hexamer into predominantly the dimer in the Gdn·HCl concentration range of 0.25−1.0 M. At higher concentrations of Gdn·HCl, the population of monomeric species increased, as evidenced by the transformation of the small shoulder at 15.0 mL into the dominant peak. The existence of separate peaks for the monomer and dimer reflects the slow dissociation (compared to the time of chromatographic separation) of dimers into monomers. Figure 3A also shows that at 2.0 M Gdn·HCl there is an equal population of dimeric and monomeric species. Above 3.5 M Gdn·HCl, insulin exists essentially as the monomer. Figure 3B shows the dependence of the elution profile on protein concentration at 2.0 M Gdn·HCl, and gives further support for the existence of an equilibrium between dimers and monomers. From Figure 3B, the population of dimer increases from 31% at 0.5 mg/mL insulin to 49.5% at 10 mg/mL. These observations also suggest that there is some dissociation of dimer into monomer during the chromatography.

The data could further be analyzed in terms of elution volume and relative area of different peaks. The position of the peaks reflects the hydrodynamic radius of a given conformer, whereas the relative area reflects its population. Figure 4A shows the elution volumes corresponding to monomers and dimers as a function of Gdn·HCl concentration. As the Gdn·HCl concentration increases, the size of the dimer undergoes a transition between 0.5 and 2.5 M from

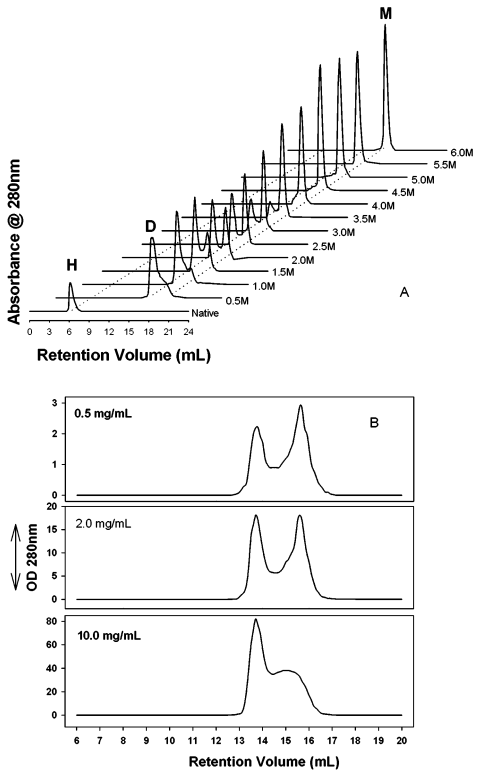

FIGURE 3: Changes in the association state and compactness of insulin as a function of Gdn·HCl concentration. Absorbance profiles from size-exclusion chromatography experiments with insulin (2 mg/mL) in varying concentrations of Gdn·HCl at pH 7.4. (A) Changes in the oligomeric state and compactness. The numbers represent the Gdn·HCl concentration. H represents hexamer, D dimer, and M monomer. (B) SEC profiles obtained after incubating 0.5, 2.0, and 10.0 mg/mL insulin in 2.0 M Gdn·HCl for 2 h prior to injection onto the column. The fraction of dimer (as a percentage), obtained from the peak areas, was 31.0% for 0.5 mg/mL, 44.9% for 2.0 mg/mL, and 49.6% for 10.0 mg/mL.

a compact to an expanded form (D_{exp}), with a midpoint at 1.5 M Gdn·HCl. No dimer was observed above 3.5 M Gdn·HCl. The size of the monomer exhibited two transitions (Figure 4A) with midpoints at 1.5 and 4.5 M for the first and second transitions, respectively. This gives rise to three sets of species: compact monomer (M_C), expanded monomer (M_{exp}), and unfolded monomer (M_U). The first transition is cooperative; the second is very broad. Note that at relatively low Gdn·HCl concentrations (between 1 and 2 M) both the compact and expanded dimer and the compact and expanded monomer coexist.

The population of monomers was calculated from the relative monomer peak areas as a function of Gdn·HCl concentration (Figure 4B). The data show two transitions, comparable to those found in the elution volume profile (Figure 4A). The first transition (C_m = 1.5 M Gdn·HCl) reflects the appearance of the expanded monomer, whereas the second transition (C_m = 3.5 M) corresponds to the dissociation of expanded monomers to unfolded monomers. In summary, SEC (Figures 3 and 4) shows the existence of at least six species differing in conformation and oligomeric state (hexamer, compact and expanded dimers, and compact, expanded, and unfolded monomers), in accord with, and complementing, the results from the circular dichroism studies.

Structural Changes in Insulin Induced by Gdn·HCl at pH 7.4 Monitored by Small-Angle X-ray Scattering. SAXS is

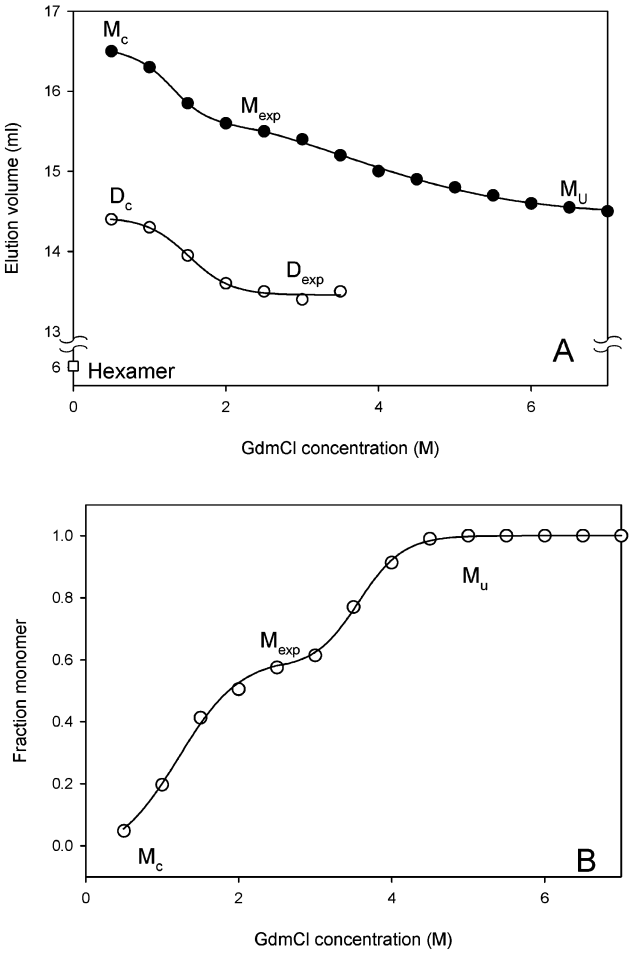

FIGURE 4: Changes in the size of insulin as a function of Gdn·HCl at pH 7.4, monitored by SEC. (A) Gdn·HCl concentration dependence of the positions of monomer peaks (●) and dimer peaks (○). (B) Fraction of monomer as a function of Gdn·HCl concentration. D refers to dimer and M to monomer, and subscripts exp and c refer to expanded and compact, respectively.

one of a few techniques that provide information about the ensemble distribution of molecular size, shape, compactness and packing (globularity), and oligomeric state (*35*). For proteins, the data can be analyzed in the form of a Kratky plot, a Guinier plot, and distance distribution [*P*(*r*)] (*32*, *35*, *36*). Insulin (4 mg/mL) was incubated for 2 h at pH 7.4 in the presence of the desired Gdn·HCl concentration before the SAXS measurements were taken. This was the lowest concentration of insulin that could be studied considering the instrumental limitations. The Kratky plot (Figure 5A) of hexameric insulin shows a compact bell-shaped Gaussian curve at lower angles, characteristic of a compactly folded globular protein. At 0.5 M Gdn·HCl, the intensity of the signal decreases, suggesting a decrease in the concentration of the large compact species due to dissociation into smaller species. The intensity of the peak at smaller angles shows a further decrease with increasing Gdn·HCl concentration, and at 6.0 M a linear profile, characteristic of unfolded protein, is observed in the Kratky plot. This suggests that insulin at lower concentrations of Gdn·HCl retains tightly packed structure even after dissociation, i.e., compact dimers and monomers. Dissociation of the hexamer into smaller oligomers is expected to be accompanied by changes in the position of the scattering maximum, as observed. Since the

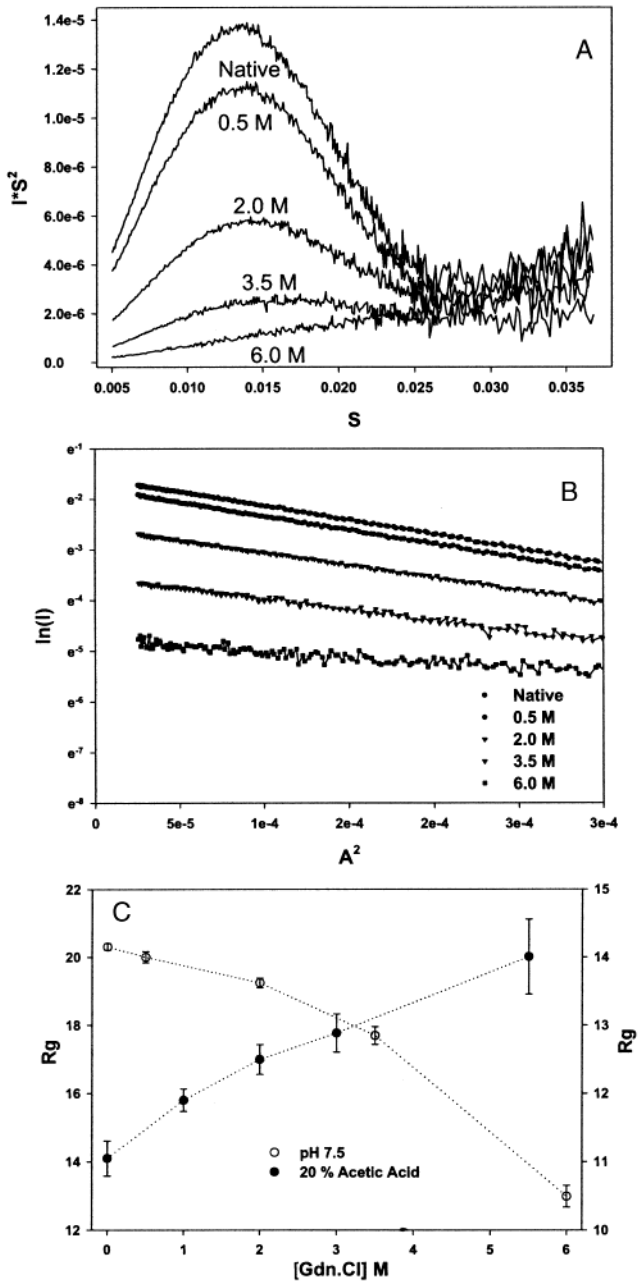

FIGURE 5: Small-angle X-ray scattering (SAXS) of insulin as a function of Gdn·HCl concentration. (A) Kratky plots at pH 7.4. (B) Guinier plots at pH 7.4. (C) Plot of R_g *vs* Gdn·HCl concentration calculated for hexamer (pH 7.4) (○) and monomer (20% acetic acid) (●). The insulin concentration was 4.0 mg/mL, and Gdn·HCl concentrations are shown beside the curves.

protein concentration for the SAXS measurements was much higher than that for the SEC experiments (due also to dilution on the column), the equilibrium is expected to be shifted to higher levels of dimer (see Figure 3B) in the SAXS measurements. At high Gdn·HCl concentrations (≥6.0 M), insulin is predominantly in the unfolded monomeric form according to SAXS.

Figure 5B shows the corresponding Guinier plots, from which the radius of gyration (R_g) can be calculated. The results are summarized in Figure 5C. The R_g of native insulin at pH 7.4 is 20.3 Å. This value is consistent with that reported previously (*31*), and corresponds to the native hexameric state of insulin. A monotonic decrease in R_g is observed as the

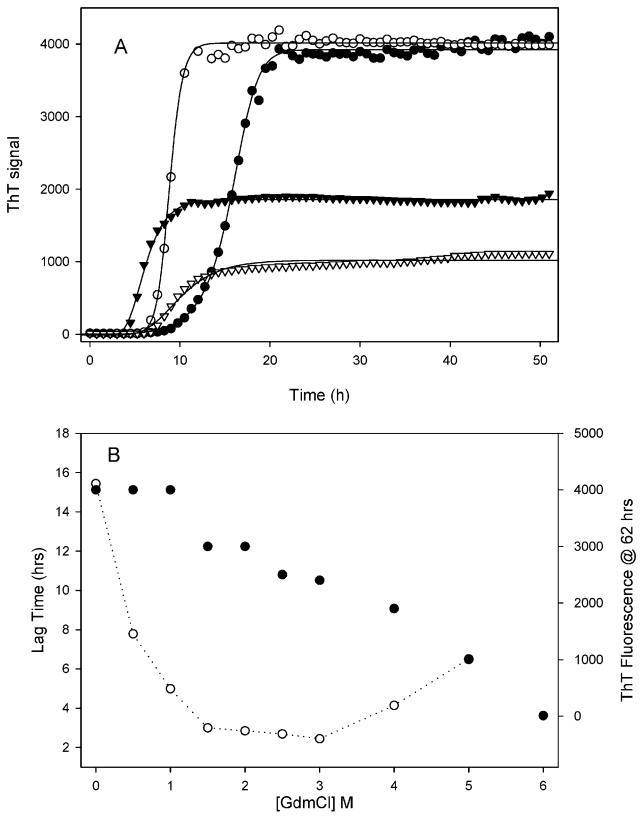

FIGURE 6: Kinetics of insulin fibrillation at pH 7.4, monitored by thioflavin T fluorescence. (A) Representative profiles of the fibrillation obtained by following ThT fluorescence: native hexameric insulin (●), 0.5 M Gdn·HCl (○), 4.0 M Gdn·HCl (▼), and 5.0 M Gdn·HCl (▽). The traces shown are the averages of more than three individual wells under each condition. (B) Dependence of the lag time (○), and the final ThT fluorescence signal (62 h) (●), on Gdn·HCl concentration. The lag time was obtained from curve fitting the average profiles at each Gdn·HCl concentration (*16*).

Gdn·HCl concentration is increased, and is attributed to progressive dissociation of insulin from hexamer to monomer. At 6.0 M Gdn·HCl, the R_g (12.8 Å) is larger than that of monomeric insulin (11.0 Å) and reflects the larger size of the unfolded monomer.

Kinetics of Fibrillation Starting with Hexameric Insulin. The involvement of structural changes leading to fibrillation is widely accepted, and it is generally believed that partially folded intermediates are critical for fibrillation (*4*, *37*). To correlate the association and conformational states of insulin, characterized above, with the propensity to fibrillate, the fibrillation was monitored as a function of Gdn·HCl concentration, starting with the hexamer.

Fibrillation of 2 mg/mL insulin at pH 7.4 was carried out at 40 °C with agitation. Studies performed at 37 and 25 °C exhibited longer lags but similar kinetic patterns (data not shown). The kinetics of fibrillation in the presence and absence of Gdn·HCl monitored by thioflavin T fluorescence are summarized in Figure 6. Similar kinetic profiles were observed when the fibrillation was monitored by light scattering (data not shown). Representative curves in Figure 6A follow a sigmoidal pattern representing an initial lag phase, an exponential growth phase, and a final plateau phase, corresponding to nucleation, extension, and equilibrium phases, respectively. Figure 6B represents the lag times calculated from curve fitting as a function of Gdn·HCl concentration. The lag time decreased from 16 h for native hexamer to 7.8 h in 0.5 M Gdn·HCl, indicating faster nucleation for the dissociated species, consistent with rate-limiting dissociation of the hexamer in fibrillation under physiological conditions. The lag time decreased almost 8 times as compared to the native value between 1.5 and 3.0 M Gdn·HCl, and then increased again above 3.0 M Gdn·HCl. Thus, the profile shows three patterns: an increased rate of fibrillation between 0 and 1.5 M, a stable region with almost the same fibrillation kinetics between 1.5 and 3.0 M, and a region above 3.0 M where the rate of fibrillation decreases.

The amount of fibrils formed, as a function of Gdn·HCl, as measured by the final ThT fluorescence signal, decreased steadily as the denaturant concentration increased (Figure 6B). This observation was supported by quantification of the protein in the supernatant at the end of the transition into fibrils at each Gdn·HCl concentration in the presence and absence of ThT (see Experimental Procedures). The results show that after incubation at 37 or 40 °C and pH 7.4, almost all the insulin is present in the insoluble fibrils at Gdn·HCl concentrations of up to 3.0 M. As the concentration of Gdn·HCl increases above 3 M, the amount of soluble protein increases (see Figure 13A). At 6.0 M Gdn·HCl, ~70% of the protein is in the soluble fraction; thus, ~30% of insulin is fibrillar under these strongly denaturing conditions. The decrease in the yield of fibrils at high concentrations of Gdn·HCl is attributed to a combination of the decreased concentration of partially folded intermediate protein present (see below and Figure 13B) and the limited solubility of insulin fibrils in high concentrations of Gdn·HCl. In independent experiments, we demonstrated that 6.4 M Gdn·HCl will partially dissolve preformed fibrils; for example, after incubation for as little as 45 min, 25% of the protein was in the supernatant, consistent with an equilibrium between soluble and insoluble fibrils of ~25:75, as observed.

Comparison of the rate of fibril formation with the changes in structure suggests that the dissociation of the hexamer has a profound effect on the rate of insulin fibrillation, and is, in fact, the rate-limiting step. Further, the rate of fibrillation was maximal between 1.5 and 3.5 M Gdn·HCl, conditions where the predominant species is the expanded monomer. Above 3.0 M Gdn·HCl, the monomer begins to unfold, resulting in the observed decrease in the rate of fibrillation, due to the decreased concentration of the critical partially folded intermediate M_{exp}. The fibrillation properties of insulin as a function of Gdn·HCl concentration were similar when the incubation was carried out at 25 °C (data not shown), except for much slower rates. Thus, the maximal rate of fibrillation in the vicinity of 2−3 M Gdn·HCl is consistent with the expanded monomer being the critical amyloidogenic intermediate in fibrillation. This conclusion is supported by the data reported below, starting with monomeric insulin, and also by experiments in which the association state and conformation of insulin during incubation at 40 °C in 2.0 M Gdn·HCl were monitored by SEC as a function of the time of incubation. These results thus indicate that structural changes affect the kinetics of fibrillation of insulin, and strongly suggest that the expanded monomer is the critical species from which the fibrils arise.

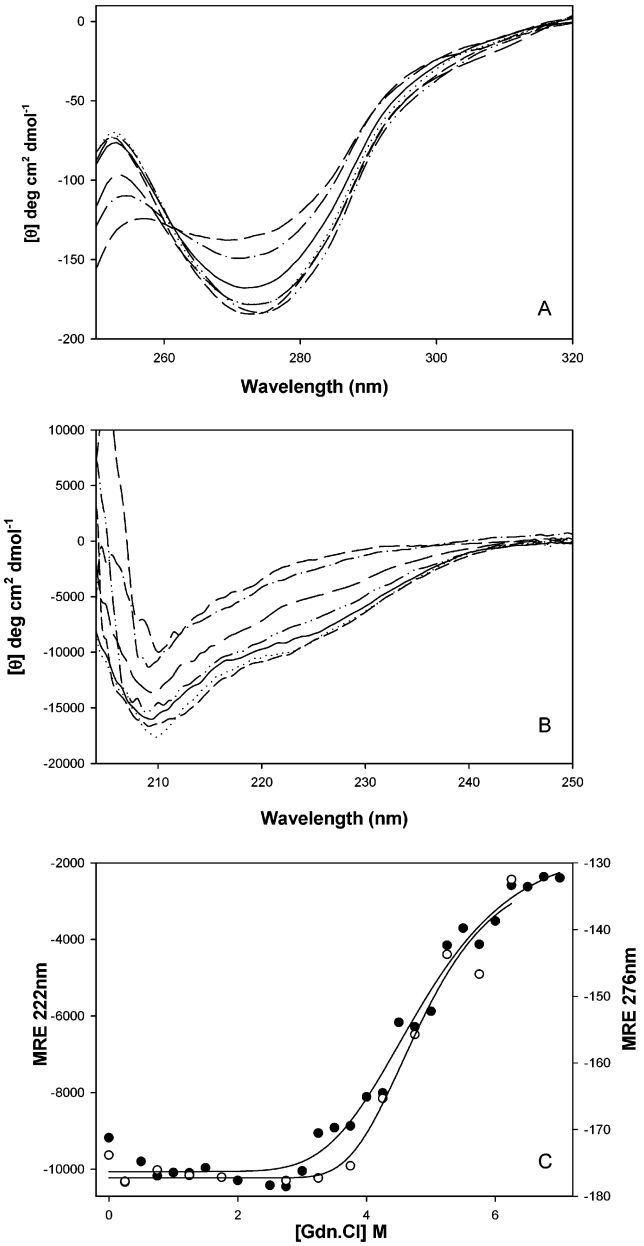

FIGURE 7: Effect of Gdn·HCl on monomeric insulin, monitored by circular dichroism. Panel A shows selected near-UV CD spectra, panel B selected far-UV CD spectra, and panel C the Gdn·HCl concentration dependence of ellipticity at 222 (●) and 276 nm (○). Conditions were as follows: 2.0 mg/mL insulin, 20% acetic acid, pH 2.0, and 25 °C. Each spectrum is the average of two independently collected spectra. In panel A, the Gdn·HCl concentrations are, from bottom to top, 0, 0.075, 1.25, 2.25, 3.25, 4.25, 5.25, and 6.25 M. In panel B, the Gdn·HCl concentrations are, in order of decreasing ellipticity at 222 nm, 0, 1.0, 2.0, 4.0, 5.0, 6.0, and 6.75 M.

Structural Changes of Monomeric Insulin. In 20% acetic acid (pH 2.0), insulin exists as a monomer (*33*, *38*). Figure 7A shows near-UV CD spectra of insulin measured in the presence of 20% acetic acid and various Gdn·HCl concentrations. After a small but reproducible enhancement in the negative ellipticity at 276 nm on the initial addition of Gdn·HCl, no further significant changes were observed up to 3.25 M Gdn·HCl, at which point the major transition starts (Figure 7C). The far-UV CD spectra (Figure 7B) show a small increase in the helical content upon addition of up to 1.0 M

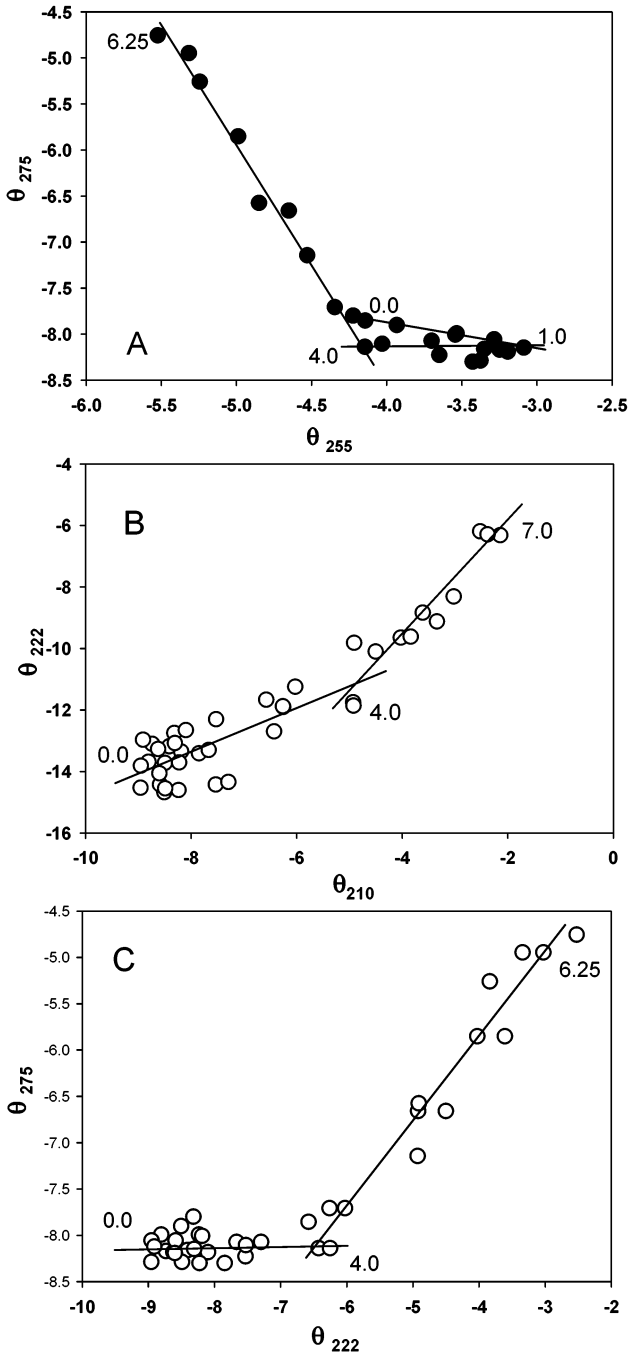

FIGURE 8: Phase diagrams for monomeric insulin from near- and far-UV CD data. (A) Changes in the near-UV CD, (B) changes in the far-UV CD, and (C) simultaneous changes in both far- and near-UV CD. See the legend of Figure 2 for details.

Gdn·HCl, which is evident from the increase in negative ellipticity at 222 nm. As with the near-UV CD, the main unfolded transition begins around 3 M Gdn·HCl; within experimental error, the near- and far-UV CD transitions are superimposable (Figure 7C). At 7.0 M Gdn·HCl, both the near- and far-UV CD spectra do not fully resemble those of the completely unfolded protein. This may reflect residual structure in the B chain helix (*34*).

To further analyze the data, phase diagrams were obtained by plotting corresponding ellipticities for both near- and far-UV CD (Figure 8). In the near-UV portion (Figure 8A), three linear segments (0−1.0, 1.0−4.0, and 4.0−6.25 M) suggest the occurrence of three different conformational transitions,

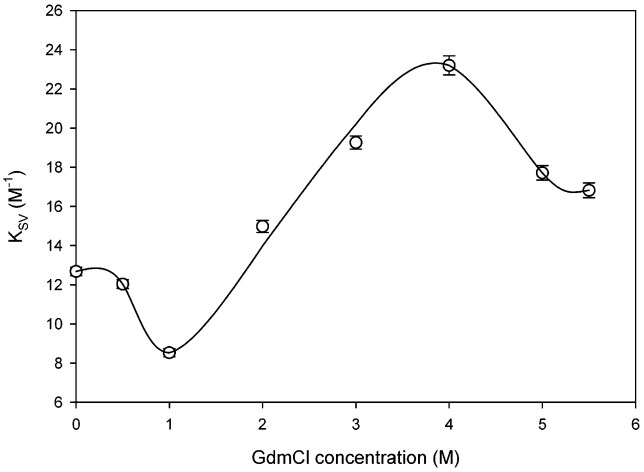

FIGURE 9: Fluorescence quenching of monomeric insulin fluorescence by acrylamide in Gdn·HCl. The plot shows the variations in the Stern−Volmer quenching constant (K_{sv}) with increases in Gdn·HCl concentration. The data were fitted to the Stern−Volmer equation to obtain K_{sv}.

and a total of four different conformational states, attributed to the compact monomer, a minor conformational change in the compact monomer, the expanded monomer, and the unfolded monomer. The far-UV phase diagram (Figure 8B) exhibits only two transitions (0−4.0 and 4.0−6.2 M), corresponding to transformations among the compact, expanded, and unfolded monomers. Interestingly, Figure 8C shows the existence of at least two different conformational transitions where changes in both secondary and tertiary structure occur simultaneously. The results, therefore, show the existence of complex structural changes taking place in the insulin monomer as a function of Gdn·HCl.

Acrylamide Quenching of Monomeric Insulin. Further proof of the structural changes taking place in the monomer with the increase in Gdn·HCl concentrations was obtained from fluorescence quenching experiments. Quenching constants (K_{sv}) were obtained by fitting the data to the Stern−Volmer equation (*39*). The resulting values of K_{sv}, plotted as a function of Gdn·HCl concentration, are summarized in Figure 9. A decrease in K_{sv} between 0 and 1.0 M suggests restricted accessibility for tyrosines under this condition. This is consistent with the increase in the near-UV CD signal under comparable conditions (Figure 7A), and is attributed to a salt effect (increased chloride ion concentration), resulting in a "tighter" monomer conformation. As three of the four tyrosines of insulin are located in helices, the observation of decreased tyrosine accessibility is consistent with the far-UV CD data that show an increased helix level in this range of Gdn·HCl concentrations. Above 1.0 M Gdn·HCl, the increase in K_{sv} reflects increased accessibility of tyrosines, reflecting the increasing level of unfolding of the molecule as the molecule transforms into the expanded form. The change in Tyr accessibility above 4 M Gdn·HCl occurs in the region where the expanded monomer becomes unfolded, and represents the partial sheltering of the tyrosine residues in the residual structure.

Small-Angle X-ray Scattering of Monomeric Insulin. The Kratky plots obtained in 20% acetic acid and different Gdn·HCl concentrations are shown in Figure 10A. The plot for the insulin monomer shows a broad bell-shaped Gaussian curve, indicative of a compact protein, although not as tightly

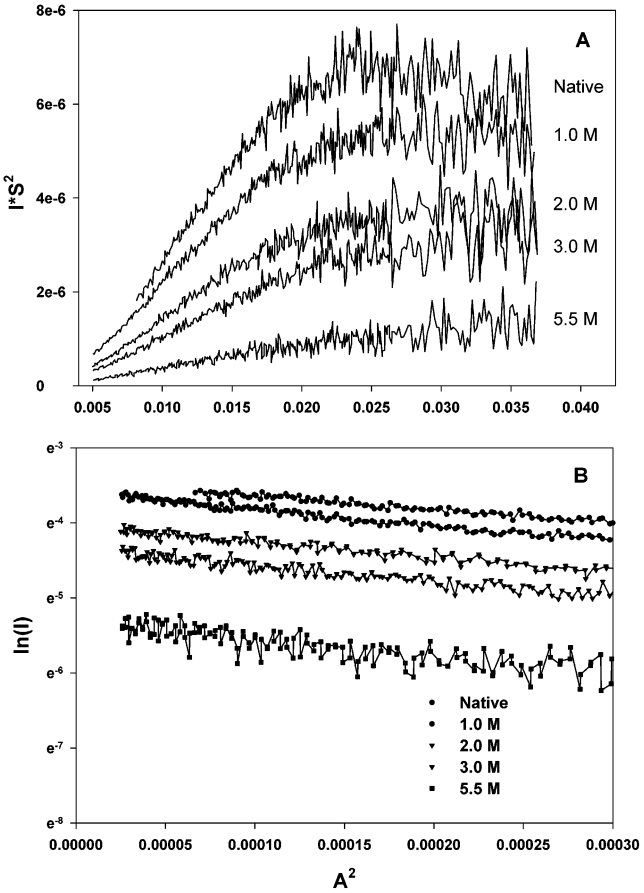

FIGURE 10: Small-angle X-ray scattering of insulin as a function of Gdn·HCl concentration in the presence of 20% acetic acid. Data were obtained as described in the legend of Figure 5, except for the use of 20% acetic acid in place of pH 7.4 buffer: (A) Kratky plots and (B) Guinier plots.

packed as in the hexamer (*31*). The addition of increasing Gdn·HCl concentrations results in a decrease in the intensity and flattening of the profiles. At 5.5 M Gdn·HCl, the plot becomes linear, consistent with the appearance of an unfolded protein. The R_g value of insulin in 20% acetic acid in the absence of denaturant (obtained from the Guinier plot, Figure 10B) was estimated to be 11.1 Å, which is consistent with that reported for the monomeric form of insulin (*31*). As the Gdn·HCl concentration was increased, an increase in R_g was observed, reaching a maximum of 14.4 Å at 5.5 M. Note that this value is somewhat larger than the R_g measured for unfolded insulin at pH 7.4 (Figure 5C), suggesting that in 20% acetic acid, Gdn·HCl unfolds the protein to a greater extent.

Fibrillation of Monomeric Insulin. Representative data for fibrillation, monitored by ThT fluorescence, from incubation of 2 mg/mL insulin in the presence of 20% acetic acid at 40 °C and different concentrations of Gdn·HCl, are shown in Figure 11A. The curves again show an initial lag phase followed by an exponential growth phase and a final equilibrium phase. The fibrillation of insulin in the presence of low concentrations of Gdn·HCl ($\leq$2 M) was significantly faster than in the absence of denaturant; in fact, the lag was essentially absent in the 0.5−1.5 M Gdn·HCl region. At higher Gdn·HCl concentrations, the lag time increased significantly above that in the absence of denaturant. The variation in the midpoints of the ThT transition *versus* Gdn·HCl concentration is shown in Figure 11B. As shown in

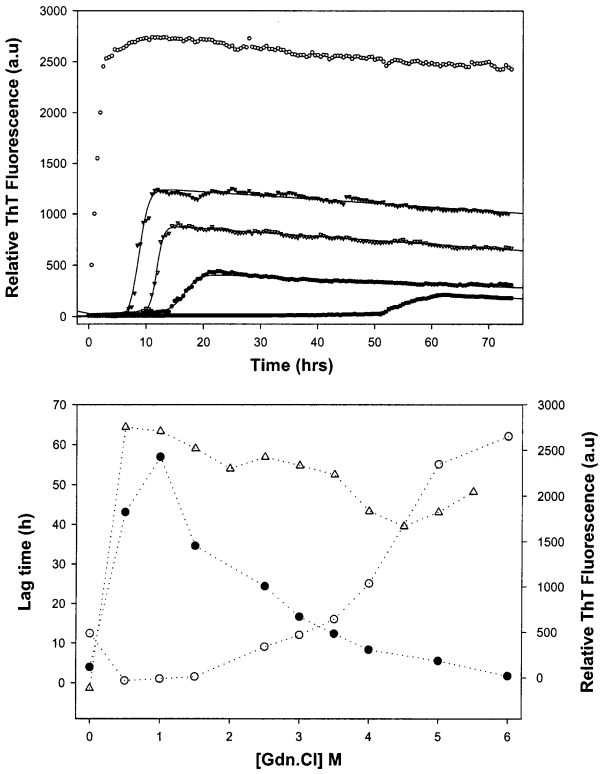

FIGURE 11: Kinetics of insulin fibrillation in 20% acetic acid, monitored by thioflavin T fluorescence. (A) Representative profiles of the fibrillation obtained by following ThT fluorescence: control 0 M Gdn·HCl (●), 1.0 M Gdn·HCl (○), 2.5 M Gdn·HCl (▼), 3.0 M Gdn·HCl (▽), and 5.0 M Gdn·HCl (■). The traces shown are the averages of more than three individual wells under each condition. (B) The dependence of the lag time (○), and the final ThT fluorescence signal (72 h) (●), on Gdn·HCl concentration. The lag time was obtained from curve fitting the average profiles at each Gdn·HCl concentration (*16*).

Figure 11B, the amount of fibrils, as measured by ThT fluorescence, varied with Gdn·HCl concentration, as observed at pH 7.4, revealing maximal fibril formation in the Gdn·HCl concentration range of 0.5−1.5 M.

Representative EM pictures of insulin fibrils grown in the presence of Gdn·HCl at pH 7.4 and 2.0 are shown in Figure 12. Fibrils in the presence and absence of Gdn·HCl have the same width (10−12 Å) but vary significantly in length and "stickiness". With both hexamer and monomer at the beginning, the presence of increasing Gdn·HCl concentrations decreased the length of the fibrils, led to increased clumping of fibrils, and made the fibrils more crystalline in appearance.

DISCUSSION

A large number of diverse diseases are now recognized as being caused by the presence of a non-native protein conformation (*40*). It is also generally accepted that pathological protein aggregation and fibril formation involve the critical intermediacy of partially folded intermediate conformations (*37*). In this study, we have analyzed the effects of the association state and conformation of insulin on its fibrillation. Equilibrium intermediate conformations were generated by destabilizing the protein using Gdn·HCl (*22*, *41*). Starting states of insulin were the hexamer at pH 7.4, its physiological state, and the monomer, which has been shown to be the stable state in 20% acetic acid (*24*, *31*).

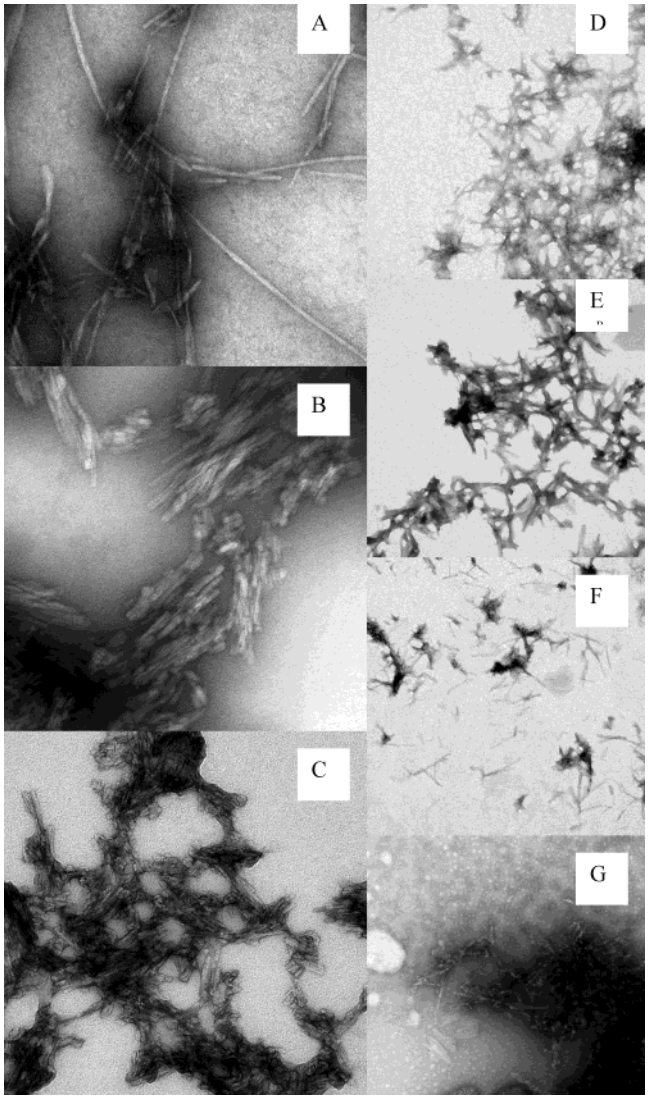

FIGURE 12: Electron micrograph images of insulin fibrils. The images show the morphology of fibrils at various Gdn·HCl concentrations in the presence of 20% acetic acid [(A) control, (B) 1.0 M Gdn·HCl, and (C) 6.0 M Gdn·HCl] and at pH 7.4 [(D) control, (E) 1.0 M Gdn·HCl, (F) 3.0 M Gdn·HCl, and (G) 5.0 M Gdn·HCl)].

Effects of Gdn·HCl on Insulin at pH 7.4. The overall picture of the structural changes induced by Gdn·HCl in human insulin at pH 7.4, as monitored by the different techniques used in this study, is given in Figure 13. In Figure 13A, the changes in the near- and far-UV CD and SEC data are plotted as a fraction of various associated signals against denaturant concentration. This information, along with that in Figure 4, was used to construct Figure 13B which shows the Gdn·HCl-induced changes in insulin structure summarized in the form of a plot of the fractions of the different states (see Scheme 1) as a function of Gdn·HCl concentration. The compact dimer is the major species at low Gdn·HCl concentrations (<2 M). In the vicinity of 1.5−5 M Gdn·HCl, the major species are the expanded dimer and monomer. At higher concentrations, the predominant species is the unfolded monomer.

Thus, the Gdn·HCl-induced denaturation of insulin is a multistage process, summarized in Scheme 1, where H represents hexamer, D dimer, M monomer, a subscript c compact, and a subscript exp expanded.

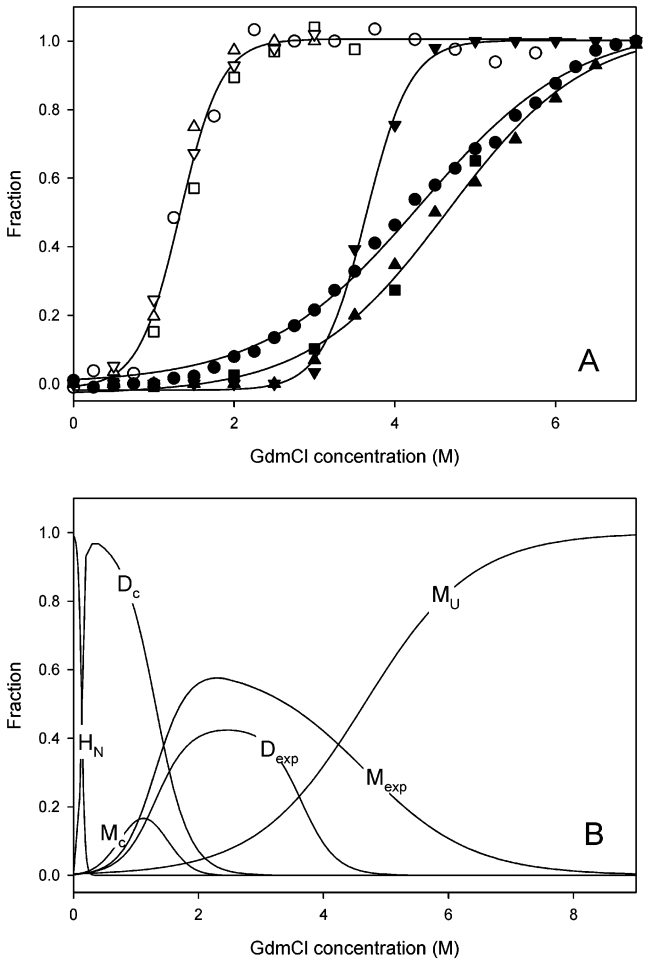

FIGURE 13: Summary of conformational changes in insulin induced by Gdn·HCl at pH 7.4. (A) Changes in near-UV CD (○), position of the peak corresponding to the dimer in SEC (□), first transition of the monomer peak position in SEC (△), first transition in the population of the monomer (▽), far-UV CD (●), second transition of the monomer position in SEC (▲), second transition in the population of the monomer (▼), and fraction soluble protein (■). (B) Fractions of each species calculated from panel A. Native hexamer (H_N), fraction of compact dimer (D_C), fraction of expanded dimer (D_{exp}), fraction of compact monomer (M_C), fraction of expanded monomer (M_{exp}), and fraction of unfolded protein (M_U). Fractions of expanded dimers and expanded monomers were calculated from SEC−HPLC data. The fraction of expanded dimers was obtained from the difference between the curve representing the decrease in the fraction of compact dimers and the curve representing the disappearance of expanded dimers (second transition in the fraction of monomers, Figure 4B). The fraction of expanded monomers was calculated from the difference between the curve representing the decrease in the fraction of compact monomers (coincident with the curve for the disappearance of compact dimers, etc.) and the curve representing unfolding (second transition in the elution volume of monomers, Figure 4A). Both fractions were scaled according to the population of monomers and dimers at 2.5 M Gdn·HCl (Figure 4B).

Scheme 1

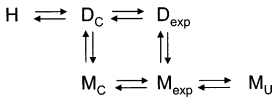

The basis for Scheme 1 follows. First, as observed by SEC, dissociation of the hexamer occurs at very low Gdn·HCl concentrations (<0.25 M); thus, the majority of the transitions observed in this study reflect changes involving the ensuing dimers and monomers. The initial changes in insulin tertiary structure at low Gdn·HCl concentrations occur simultaneously with dissociation of dimers, and expansion of dimers and monomers as detected by changes in the SEC profile and near-UV CD. These transitions happen within a narrow range of Gdn·HCl concentrations ($\Delta C \sim 1.5$ M), lead to a mixture of expanded dimer and monomer, and are characterized by a C_m of 1.3−1.5 M Gdn·HCl. The next stage represents dissociation of the expanded dimers to expanded monomers ($\Delta C \sim 1.5$ M, $C_m \sim 3.6$ M Gdn·HCl) (Figure 13B). Changes in insulin secondary structure (from far-UV CD) occur over a wide range of denaturant concentrations ($\Delta C > 4$ M), with a C_m of 4.3 M Gdn·HCl, and closely parallel the population of unfolded monomers from SEC ($C_m = 4.7$ M Gdn·HCl). Usually, changes in secondary structure occur simultaneously with the changes in protein hydrodynamic dimensions (*42*). However, there is some divergence with insulin between the unfolding curve monitored by changes in the far-UV CD and the increase in the size of the monomer corresponding to unfolding. This is due to the complex unfolding pattern of insulin, which involves multiple dissociations and multiple conformational changes.

Partially Folded Intermediates and Fibrillation from Hexameric Insulin. The SEC data at pH 7.4 reveal a total of six different states of insulin, depending on the Gdn·HCl concentration. The starting hexamer is dissociated into compact dimers at very low denaturant concentrations. This dimer simultaneously both expands and dissociates into a mixture of compact and expanded monomer at low Gdn·HCl concentrations. As the Gdn·HCl concentration is increased, the compact monomers transform into the expanded state, and eventually convert into the unfolded monomeric state. The two expanded species are distinct partially unfolded intermediates: partially folded intermediates have been previously reported for insulin, as noted in the introductory section, but the association state of spectroscopically detected intermediates was not previously ascertained. It is likely that the expanded monomer is similar to the previously reported partially folded intermediate based on spectroscopic measurements (*22*). The observation of the expanded dimer of insulin is probably the first definitive observation of such a species, i.e., a noncovalently linked dimer of partially folded subunits.

The circular dichroism data indicate a complex set of partially unfolded structures as evident by the phase diagrams at pH 7.4. At physiological pH, Gdn·HCl modifies both the secondary and tertiary or quaternary structure of insulin. At least six non-native conformations or states were observed for insulin (pH 7.4) over the whole Gdn·HCl concentration range; these are in accord with those identified by SEC. The much greater amount of information available from the phase diagram (Figure 2), relative to the traditional analysis of CD data (Figure 1C), demonstrates the advantages of this procedure.

Although the correlation of specific insulin conformations with fibrillation is complicated because of the overlap of the different states (Figure 13B), as well as the independent effect of Gdn·HCl on fibrils, leading to their dissolution, the data unequivocally demonstrate that fibrillation arises from a non-native conformation, and further are most consistent with the expanded monomer being the key conformational state

leading to fibrils. This interpretation is unambiguous for the experiments starting with monomer. Thus, we conclude that the expanded monomer is responsible for fibrillation at both neutral and low pH.

That concentrations lower than 0.5 M Gdn·HCl cause hexameric insulin dissociation into predominantly the dimeric form is consistent with this dimer being on the pathway for the assembly of the insulin hexamer. Since Gdn·HCl is a polar chaotrope, it is likely that the dimer is stabilized by strong hydrophobic interactions that endow it with significant stability to remain associated up to 3.0 M Gdn·HCl (*20*, *25*, *43*−*45*). The data also indicate that the dimer−dimer subunit interactions in the hexamer are weaker than those of the monomer−monomer subunits in the dimer. This also explains the lack of detectable tetramers in these experiments.

Partially Folded Intermediates and Fibrillation of Monomeric Insulin. To remove the complexity of the interpretation of data at pH 7.4 due to the contribution of associated oligomeric species, we carried out studies on the monomeric form of insulin in 20% acetic acid (*33*, *38*). CD, fluorescence quenching, and SAXS studies demonstrate the existence of multiple conformations and varying degrees of unfolding under these conditions.

At low concentrations, between 0 and 1 M Gdn·HCl, a small increase in the helical content of insulin was observed by CD, which was supported by quenching studies showing reduced accessibility of tyrosines, the majority of which lie in the helix region. This effect is attributed to a salt effect due to the increased concentration of chloride anion, and has been observed previously in other systems (*46*, *47*). These low concentrations of Gdn·HCl significantly increased the kinetics of insulin fibrillation; this effect is attributed to the increased ionic strength, rather than the small conformational change, since we have shown that the kinetics of insulin fibrillation are very dependent on ionic strength (*16*). Between 1 and 4 M Gdn·HCl, the compact monomer of insulin undergoes a transition, observed by near- and far-UV CD, acrylamide quenching, and SAXS, into an expanded partially folded intermediate, which appears to be the major species responsible for fibrillation. All these techniques indicate that there are only three detectable major monomeric species of insulin, the two forms of the compact monomer, the expanded monomer, and the unfolded monomer. The data indicate that the latter is not fully unfolded, but retains some residual structure. The smaller amount of fibrils, and decreased rate of fibrillation, at high Gdn·HCl concentrations are ascribed to two phenomena: the increasing amount of unfolded insulin means that the concentration of the fibrillating species is decreased, leading to slower kinetics (since the rate of fibrillation is proportional to the protein concentration), and the high concentrations of denaturant cause some dissolution of the fibrils. Despite these constraints, fibrils were observed up to 5.5 M Gdn·HCl, reflecting the low concentrations of expanded monomer present.

The results reported here are similar in some respects to those recently reported for the formation of fibrils from β-lactoglobulin in the presence of urea (*48*). For β-lactoglobulin, the urea concentration where fibril formation is most rapid, for both seeded and unseeded solutions, is approximately 5.0 M, close to the concentration of urea corresponding to the midpoint of unfolding. This suggests that fibril formation arises from a significantly unfolded conformation, as is the case with insulin, and other amyloidogenic proteins, such as immunoglobulin light chains (*49*).

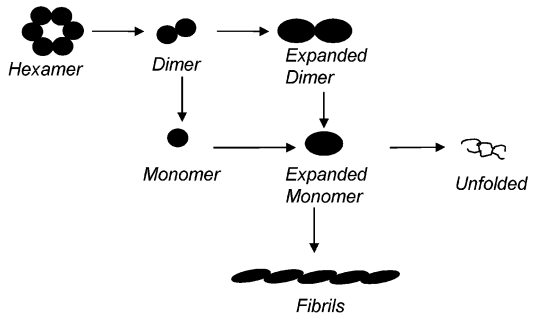

FIGURE 14: Model showing the major species of insulin present in Gdn·HCl-induced fibril formation. A similar model is assumed to apply in the absence of the denaturant.

CONCLUSIONS

As with transthyretin (*50*, *51*), a tetramer that forms amyloid fibrils in several diseases, our data indicate that fibrillation of insulin requires dissociation to monomer, followed by conformational change to form a critical amyloidogenic partially unfolded intermediate. A model for insulin fibrillation is given in Figure 14. Although this model was derived from the current study in the presence of Gdn·HCl, we believe that a similar situation will exist in the absence of the denaturant. In this case, the concentrations of the intermediate species will be significantly lower than in the presence of the destabilizing Gdn·HCl, leading to the observed slower fibrillation. The fact that fibrillation arises from the expanded monomer (partially unfolded intermediate), which lacks significant tertiary structure as well as limited secondary structure, indicates that models for fibril structure, based on the three-dimensional structure of the native state (*45*, *52*, *53*), are unlikely to be correct.

ACKNOWLEDGMENT

Small-angle X-ray scattering data were collected at beamline 4-2, Stanford Synchrotron Radiation Laboratory (SSRL). SSRL is supported by the U.S. Department of Energy, Office of Basic Energy Sciences, and in part by the National Institutes of Health, National Center for Research Resources, Biomedical Technology Program, and by the Department of Energy, Office of Biological and Environmental Research. We especially thank Dr. James Flink.

REFERENCES

1. Carrell, R. W., and Lomas, D. A. (1997) *Lancet 350*, 134−138.
2. Carrell, R. W., and Gooptu, G. (1998) *Curr. Opin. Struct. Biol. 8*, 799−809.
3. Thomas, P. J., Qu, B. H., and Pedersen, P. L. (1995) *Trends Biochem. Sci. 20*, 456−459.
4. Rochet, J. C., and Lansbury, P. T., Jr. (2000) *Curr. Opin. Struct. Biol. 10*, 60−68.
5. Uversky, V. N., Gillespie, J. R., Talapatra, A., and Fink, A. L. (1999) *Med. Sci. Monit. 5*, 1001−1012.
6. Uversky, V. N., Gillespie, J. R., Talapatra, A., and Fink, A. L. (1999) *Med. Sci. Monit. 5*, 1238−1254.
7. Sipe, J. D., and Cohen, A. S. (2000) *J. Struct. Biol. 130*, 88−98.
8. Sunde, M., and Blake, C. (1997) *Adv. Protein Chem. 50*, 123−159.
9. Zerovnik, E. (2002) *Eur. J. Biochem. 269*, 3362−3371.
10. Glenner, G. G. (1981) *Prog. Histochem. Cytochem. 13*, 1−37.
11. Blake, C., and Serpell, L. (1996) *Structure 4*, 989−998.

12. Burke, M. J., and Rougvie, M. A. (1972) *Biochemistry 11*, 2435−2439.
13. Bucciantini, M., Giannoni, E., Chiti, F., Baroni, F., Formigli, L., Zurdo, J., Taddei, N., Ramponi, G., Dobson, C. M., and Stefani, M. (2002) *Nature 416*, 507−511.
14. Soto, C. (2001) *FEBS Lett. 498*, 204−207.
15. Waugh, D. F., Wilhelmson, D. F., Commerford, S. L., and Sackler, M. L. (1953) *J. Am. Chem. Soc. 75*, 2592−2600.
16. Nielsen, L., Khurana, R., Coats, A., Frokjaer, S., Brange, J., Vyas, S., Uversky, V. N., and Fink, A. L. (2001) *Biochemistry 40*, 6036−6046.
17. Dische, F. E., Wernstedt, C., Westermark, G. T., Westermark, P., Pepys, M. B., Rennie, J. A., Gilbey, S. G., and Watkins, P. J. (1988) *Diabetologia 31*, 158−161.
18. Brange, J., Andersen, L., Laursen, E. D., Meyn, G., and Rasmussen, E. (1997) *J. Pharm. Sci. 86*, 517−525.
19. Sluzky, V., Klibanov, A. M., and Langer, R. (1992) *Biotechnol. Bioeng. 40*, 895−903.
20. Brange, J., and Langkjoer, L. (1993) *Pharm. Biotechnol. 5*, 315−350.
21. Bryant, C., Strohl, M., Green, L. K., Long, H. B., Alter, L. A., Pekar, A. H., Chance, R. E., and Brems, D. N. (1992) *Biochemistry 31*, 5692−5698.
22. Millican, R. L., and Brems, D. N. (1994) *Biochemistry 33*, 1116−1124.
23. Bouchard, M., Zurdo, J., Nettleton, E. J., Dobson, C. M., and Robinson, C. V. (2000) *Protein Sci. 9*, 1960−1967.
24. Weiss, M. A., Hua, Q. X., Lynch, C. S., Frank, B. H., and Shoelson, S. E. (1991) *Biochemistry 30*, 7373−7389.
25. Whittingham, J. L., Scott, D. J., Chance, K., Wilson, A., Finch, J., Brange, J., and Guy, D. G. (2002) *J. Mol. Biol. 318*, 479−490.
26. Naiki, H., Higuchi, K., Hosokawa, M., and Takeda, T. (1989) *Anal. Biochem. 177*, 244−249.
27. Burstein, E. A. (1976) *Intrinsic Protein Fluorescence*: *Origin and Applications*, VINITI, Moscow.
28. Permyakov, E. A., Yarmolenko, V. V., Emelyanenko, V. I., Burstein, E. A., Closset, J., and Gerday, C. (1980) *Eur. J. Biochem. 109*, 307−315.
29. Kuznetsova, I. M., Stepanenko, O. V., Turoverov, K. K., Zhu, L., Zhou, J. M., Fink, A. L., and Uversky, V. N. (2002) *Biochim. Biophys. Acta 1596*, 138−155.
30. Bushmarina, N. A., Kuznetsova, I. M., Biktashev, A. G., Turoverov, K. K., and Uversky, V. N. (2001) *ChemBioChem 2*, 813−821.
31. Uversky, V. N., Garriques, L. N., Millett, I. S., Frokjaer, S., Brange, J., Doniach, S., and Fink, A. L. (2003) *J. Pharm. Sci. 92*, 847−858.
32. Glatter, O., and Kratky, O. (1982) in *Small-angle X-ray scattering*, pp 515, Academic Press, London.
33. Nielsen, L., Frokjaer, S., Brange, J., Uversky, V. N., and Fink, A. L. (2001) *Biochemistry 40*, 8397−8409.
34. Hua, Q. X., Nakagawa, S. H., Jia, W., Hu, S. Q., Chu, Y. C., Katsoyannis, P. G., and Weiss, M. A. (2001) *Biochemistry 40*, 12299−12311.
35. Doniach, S. (2001) *Chem. Rev. 101*, 1763−1778.
36. Svergun, D. I., and Koch, M. H. (2002) *Curr. Opin. Struct. Biol. 12*, 654−660.
37. Fink, A. L. (1998) *Folding Des. 3*, 9−15.
38. Hua, Q. X., and Weiss, M. A. (1991) *Biochemistry 30*, 5505−5515.
39. Lakowicz, J. R. (1983) *Principles of Fluorescence Spectroscopy*, Plenum Press, New York.
40. Kopito, R. R., and Ron, D. (2000) *Nat. Cell Biol. 2*, E207−E209.
41. Brems, D. N., Brown, P. L., Heckenlaible, L. A., and Frank, B. H. (1990) *Biochemistry 29*, 9289−9293.
42. Uversky, V. N., and Fink, A. L. (2002) *FEBS Lett. 515*, 79−83.
43. Chang, X., Jorgensen, A. M., Bardrum, P., and Led, J. J. (1997) *Biochemistry 36*, 9409−9422.
44. Shoelson, S. E., Lu, Z. X., Parlautan, L., Lynch, C. S., and Weiss, M. A. (1992) *Biochemistry 31*, 1757−1767.
45. Yao, Z. P., Zeng, Z. H., Li, H. M., Zhang, Y., Feng, Y. M., and Wang, D. C. (1999) *Acta Crystallogr. D55*, 1524−1532.
46. Hagihara, Y., Aimoto, S., Fink, A. L., and Goto, Y. (1993) *J. Mol. Biol. 231*, 180−184.
47. Nishimura, C., Uversky, V. N., and Fink, A. L. (2001) *Biochemistry 40*, 2113−2128.
48. Hamada, D., and Dobson, C. M. (2002) *Protein Sci. 11*, 2417−2426.
49. Khurana, R., Gillespie, J. R., Talapatra, A., Minert, L. J., Ionescu-Zanetti, C., Millett, I., and Fink, A. L. (2001) *Biochemistry 40*, 3525−3535.
50. Colon, W., Lai, Z., McCutchen, S. L., Miroy, G. J., Strang, C., and Kelly, J. W. (1996) *Ciba Found. Symp. 199*, 228−238.
51. Lai, Z., Colón, W., and Kelly, J. W. (1996) *Biochemistry 35*, 6470−6482.
52. Brange, J., Dodson, G. G., Edwards, D. J., Holden, P. H., and Whittingham, J. L. (1997) *Proteins 27*, 507−516.
53. Carter, D. B., and Chou, K. C. (1998) *Neurobiol. Aging 19*, 37−40.

BI034868O